J Sol-Gel Sci Technol (2016) 78:422–429
DOI 10.1007/s10971-015-3953-4

ORIGINAL PAPER: SOL-GEL AND HYBRID MATERIALS FOR OPTICAL, PHOTONIC AND OPTOELECTRONIC APPLICATIONS

Modification of electrical and optical properties of CuO thin films by Ni doping

Silan Baturay[1] · Ahmet Tombak[2] · Derya Kaya[1] · Yusuf Selim Ocak[3,4] · Murat Tokus[1] · Murat Aydemir[3] · Tahsin Kilicoglu[1]

Received: 4 September 2015 / Accepted: 30 December 2015 / Published online: 18 January 2016

Abstract Undoped and Ni-doped CuO thin films were deposited onto glass substrates using a spin-coating technique at different doping concentrations (undoped, 2, 4, 6, and 10 %). X-ray diffraction patterns for undoped and Ni-doped CuO thin films indicated that the films were polycrystalline, with preferential growth in the (002), (111), and (−311) directions. Atomic force microscopy images revealed that the surface morphologies of the films were not uniform. Scanning electron microscopy images confirmed the presence of agglomerated particles on the surfaces; the coverage increased with the doping level. A Hall effect system with a van der Pauw configuration was used to investigate the electrical properties of the CuO films. The free charge carrier concentration decreased and hole mobility increased with increasing Ni concentration, with the exception of the 10 % Ni-doped CuO sample. Ultraviolet–visible spectroscopy measurements of the film samples indicated an average transmittance of 30–40 % in the visible range. The optical band gap decreased slightly for low-level doping and increased from 2.03 to 2.22 eV for 10 % Ni incorporation. The electrical and optical properties of the CuO films were modified by Ni doping, i.e. the band gap decreased and the mobility increased almost linearly, with the exception of the 10 % Ni-doped sample.

Graphical Abstract SEM images of **a** undoped **b** 2 % **c** 4 % **d** 6 %, and **e** 10 % Ni-doped CuO thin films.

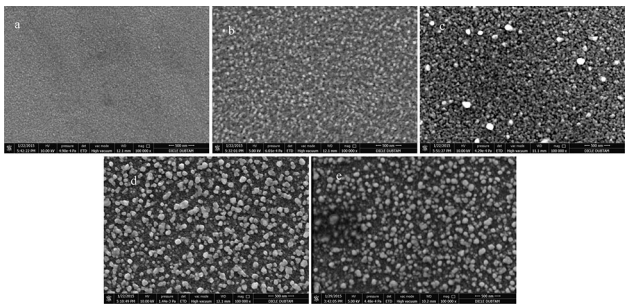

Keywords Band gap · CuO · Metal oxides · Mobility · Nickel doping · Optical properties

1 Introduction

In recent years, nanostructured CuO materials, with band gaps ranging from 1.5 to 3 eV, have been investigated due to their unique photoelectrochemical [1], electrical [2], and photoluminescence [3] properties. CuO has demonstrated its potential in solar cell [4], gas sensor [5], superconducting material [6], and antimicrobial [7] applications. The advantages of using CuO in industrial applications include its low cost, non-toxicity, and ease of manufacture. Numerous methods have been used to fabricate CuO, including pulsed laser deposition [8], spin-coating [9], thermal evaporation [10], microwave combustion [11], chemical vapour deposition [12], microwave irradiation

✉ Yusuf Selim Ocak
yusufselim@gmail.com

1 Department of Physics, Faculty of Science, Dicle University, Dicle, Turkey

2 Department of Physics, Faculty of Science, Batman University, Batman, Turkey

3 Science and Technology Application and Research Center, Dicle University, Diyarbakir, Turkey

4 Faculty of Education, Department of Science, Dicle University, Diyarbakir, Turkey

[13], successive ionic layer adsorption and reaction (SILAR) [14], molecular beam epitaxy [15], and dip-coating techniques [16]. Compared with other deposition techniques, spin-coating is especially efficient, due to its high deposition rate and low cost.

The physical and chemical properties of a CuO thin film can be affected by doping in terms of the resulting optical, electrical, and structural properties. Sonia et al. [17] reported a band gap change from 3.01 to 2.49 eV for Zn-doped CuO nanoparticles. Chand et al. [18] demonstrated a reduction in the optical band gap from 2.99 to 2.76 eV in Li-doped CuO thin films. Bayansal et al. [19] reported that Pb doping increased the band gap by 0.37 eV with respect to undoped CuO. Mohamed Basith et al. [20] showed that the optical band gap of CuO films increased with Fe doping; Fe-doped CuO exhibited ferromagnetic behaviour that was dependent on the amount of dopant (Fe^{2+}) ions. Jiang et al. [21] investigated the optical and structural properties of CuO nanosheets formed by hydrothermal methods at low temperature.

Transition metals (e.g. Ni, Ag, Li, Pb, and Bi) have been incorporated into CuO films [11, 18, 19, 22, 23]. Ni-doped CuO nanostructures with a hexagonal crystal structure exhibit ferromagnetic behaviour at room temperature, the extent to which was dependent on the amount of dopant ions [11]. Although the optical and electrical properties of doped CuO films have been investigated by researchers [9, 11, 24, 25], Ni-doped CuO films grown by spin-coating techniques have not been investigated to date. The purpose of this study was to modify the electrical and absorption properties of CuO thin films in the visible region for photovoltaic applications. With this motivation, Ni-doped CuO films were deposited on soda lime glass using a spin-coating method. The optical properties of the films were investigated using ultraviolet–visible (UV–Vis) spectroscopy. Hall effect measurements were used to reveal the electrical properties of the films. X-ray diffraction (XRD), scanning electron microscopy (SEM), and atomic force microscopy (AFM) provided information on the crystalline nature and surface morphology of the thin film samples.

2 Experimental details

Before deposition, glass substrates were cleaned by ultrasonication in acetone and methanol for 10 min. Before each step, the substrates were washed with deionised water and dried under a nitrogen atmosphere. First, 0.1 M copper (II) acetate monohydrate ($(CH_3COO)_2Cu{\cdot}H_2O$) was dissolved in 100 mL of methanol; 0.3 mL of diethanolamine was added as a stabiliser. Nickel (II) chloride hexahydrate ($NiCl_2{\cdot}6H_2O$; 0.01 M) was dissolved in 40 mL of methanol. The desired molar ratio of Cu to Ni solutions was mixed and stirred for 1 day to obtain homogenous mixtures. Ni-doped copper (II) acetate solutions were prepared in doping concentrations of 2, 4, 6, and 10 %. A five-step spin-coating process was applied to fabricate homogeneous films using a SCS G3P-8 spin-coating system. Figure 1 shows a schematic diagram of the spin-coating steps. After each spinning step, the films were heated at 250 °C for 10 min. This deposition process was repeated 10× to obtain the desired film thickness. The films were then annealed at 500 °C for 1 h in air ambient.

The crystal structures of the as-grown CuO thin films were determined using a Smart Lab XRD system (Rigaku

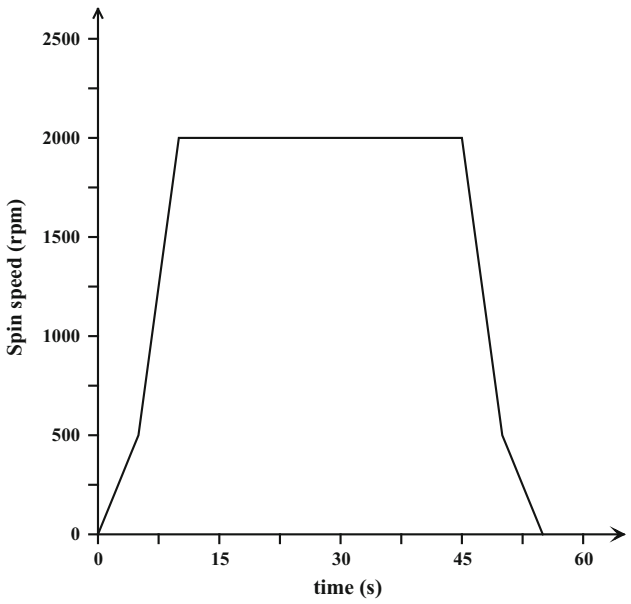

Fig. 1 Schematic view of spinning steps

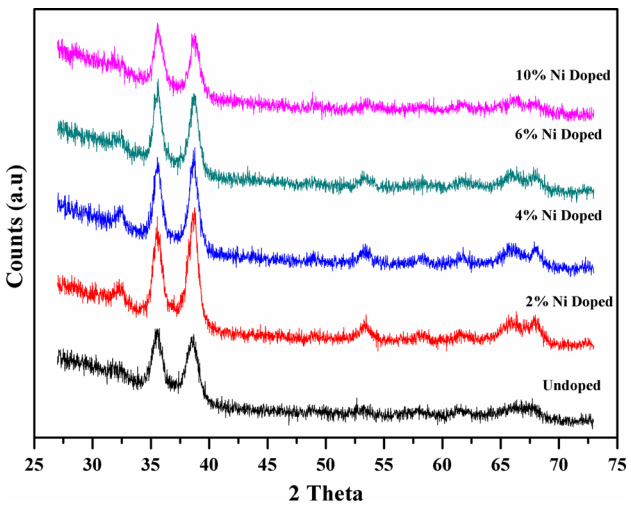

Fig. 2 XRD patterns of the films

Table 1 XRD patterns of the films

	2 Theta peaks (°)	FWHM (radians)	Grain size (nm)	d-spacing (Å)	d-spacing Ref. [27] (Å)	Orientation	Dislocation density (m^{-2})	Strain
Undoped	35.46	0.14	59.66	2.2800	2.5289	002	2.81×10^{14}	0.0333
	38.52	0.50	16.85	2.1050	2.3217	111	3.52×10^{15}	0.118
	66.10	0.26	36.51	1.2731	1.4089	−311	4.31×10^{15}	0.0545
2 % Ni-doped	32.60	0.52	15.94	2.4739	2.7499	110	3.93×10^{15}	0.125
	35.54	0.38	21.98	2.2750	2.5289	002	2.07×10^{15}	0.0905
	38.84	0.17	49.62	2.0883	2.3217	111	4.06×10^{15}	0.0401
	53.46	0.80	11.13	1.5437	1.7113	020	8.07×10^{15}	0.179
	67.96	1.05	9.13	1.2423	1.3780	113	1.20×10^{16}	0.218
4 % Ni-doped	32.58	0.26	31.88	2.4754	2.7499	110	9.84×10^{14}	0.0624
	35.58	0.30	27.85	2.2726	2.5226	−111	1.29×10^{14}	0.0714
	38.76	0.68	12.40	2.0924	2.3217	111	6.50×10^{15}	0.160
	53.4	0.52	17.12	1.5453	1.7113	020	3.41×10^{14}	0.116
	67.88	0.16	59.94	1.2436	1.3780	113	2.78×10^{14}	0.0332
6 % Ni-doped	35.64	0.80	10.44	2.2689	2.5289	−111	9.17×10^{15}	0.190
	38.66	0.58	14.53	2.0976	2.3217	111	4.74×10^{15}	0.137
	53.12	0.72	12.35	1.5528	1.7113	020	6.56×10^{15}	0.161
	67.82	1.55	6.16	1.2446	1.3780	113	6.64×10^{16}	0.322
10 % Ni-doped	35.82	0.34	24.59	2.2578	2.5226	−111	1.65×10^{15}	0.0809
	38.88	0.48	17.57	2.0862	2.3217	111	3.24×10^{14}	0.113

Corporation, Tokyo, Japan; Cu-Kα radiation; λ 1.540056 Å) for phase purity analysis. The surface morphology of the Ni-doped CuO films was investigated using an XE 100 atomic force microscope (Park Systems Corp., Suwon, Korea) and a Quanta FEG 250 scanning electron microscope (FEI Co., Eindhoven, The Netherlands). A UV-3600 spectrophotometer (Shimadzu, Tokyo, Japan) was used to record the absorbance and transmittance properties of the films. The film's electrical properties, and the charge carrier concentration, mobility, conductivity type, and resistivity, were measured with an HMS 3000 Hall measurement system (Ecopia, Gyeonggi-do, South Korea).

3 Results and discussion

3.1 XRD analysis

Figure 2 shows a typical XRD pattern for undoped and Ni-doped films deposited on glass substrates annealed at 500 °C. Strong peaks at 35.4° and 38.5° and a low-intensity peak at 66.8° were associated with reflections from the (002), (111), and (−311) planes, respectively. The XRD patterns showed that the films were polycrystalline in nature, with a tenorite structure. The peak positions, grain sizes in nanometres, interplanar spacing, and full width at half maximum (FWHM) values are listed in Table 1, along with corresponding values from Ref. [26] for comparison. Slight differences were observed in the peak positions; however, the intensities of the peaks corresponding to the (002) and (111) orientations were high. As the doping ratio increased, the intensities of the weak peaks (e.g. at 32°, 67°, and 53°) decreased and disappeared completely for the 10 % Ni-doped film sample. Ni addition did not change the crystal structure significantly. The atomic radius of the Ni^{+2} ion (0.69 Å) is close to that of the Cu^{+2} ion (0.73 Å). Thus, an exchange of Cu and Ni ions should preserve the crystal structure. This was confirmed in XRD data; no peaks corresponding to metallic Cu or Ni in the Ni-doped CuO films were observed. Scherrer's equation was used to evaluate the grain sizes of Ni-doped and undoped CuO films from the XRD patterns. Scherrer's equation is given as follows:

$$D = \frac{K\lambda}{\beta \cos\theta} \quad (1)$$

where D is the mean crystallite size, $\lambda = 1.540056$ Å is the wavelength of Cu-Kα irradiation, β is the FWHM, θ is the Bragg's diffraction angle, and K is the shape factor ($K = 0.89$). As the doping concentration increased, the calculated average grain size for the strong peaks decreased from 38 to 12 nm, with the exception of that for the 10 % Ni-doped thin films; the calculated average grain size for the 10 % Ni-doped CuO films was 21 nm. This shows that

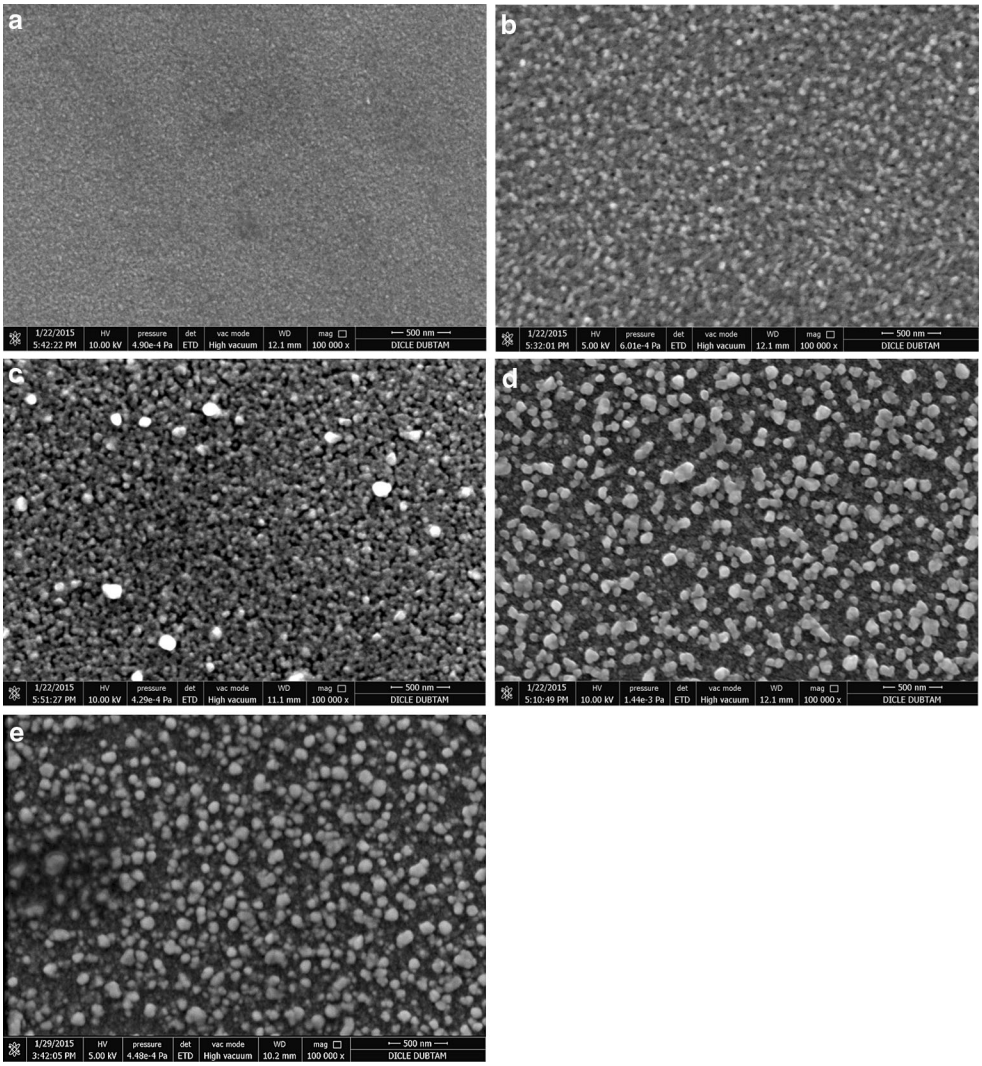

Fig. 3 SEM image of **a** undoped CuO film, **b** 2 % Ni-doped CuO film, **c** 4 % Ni-doped CuO film, **d** 6 % Ni-doped CuO film, **e** 10 % Ni-doped CuO film

the grain size of all films changes with the Ni content. The average grain size decreased for 2, 4, and 6 % Ni-doped thin films because of the improvement in crystallinity of CuO films and ionic radii difference between Cu^{2+} and Ni^{2+}. The average grain size increased for 10 % Ni-doped thin films by increasing the molecular concentration at the crystal surface. d values of the all thin films can be calculated using the Bragg's equation:

$$2d\sin\theta = n\lambda \tag{2}$$

where n is the order of diffraction, λ is the wavelength of the XRD, and θ is the angle of diffraction. The dislocation density (δ), which gives the amount of defects in the crystal, is estimated using the relation:

$$\delta = \frac{1}{D^2} \tag{3}$$

where D is the crystallite size. Strain (ε) of the obtained films is calculated from the following relation [27]:

$$\varepsilon = \frac{\beta\cos\theta}{4} \tag{4}$$

where β is the full width at half maximum (FWHM) in radians. Table 1 gives the grain size, dislocation density, and strain for undoped and Ni-doped CuO thin films. The calculated dislocation densities in our case increased from 9.84×10^{14} to 2.64×10^{16} with increase in Ni concentration. It was observed that the lattice spacing value of the preferential orientation of the films changed with different Ni concentrations which may be attributed to the evidences of strain in Ni-doped CuO films. From these results, it was confirmed that the fundamental effect of increase in crystallite size is related to decrease in strain. The decrease in strain indicates the decrease in lattice imperfections and

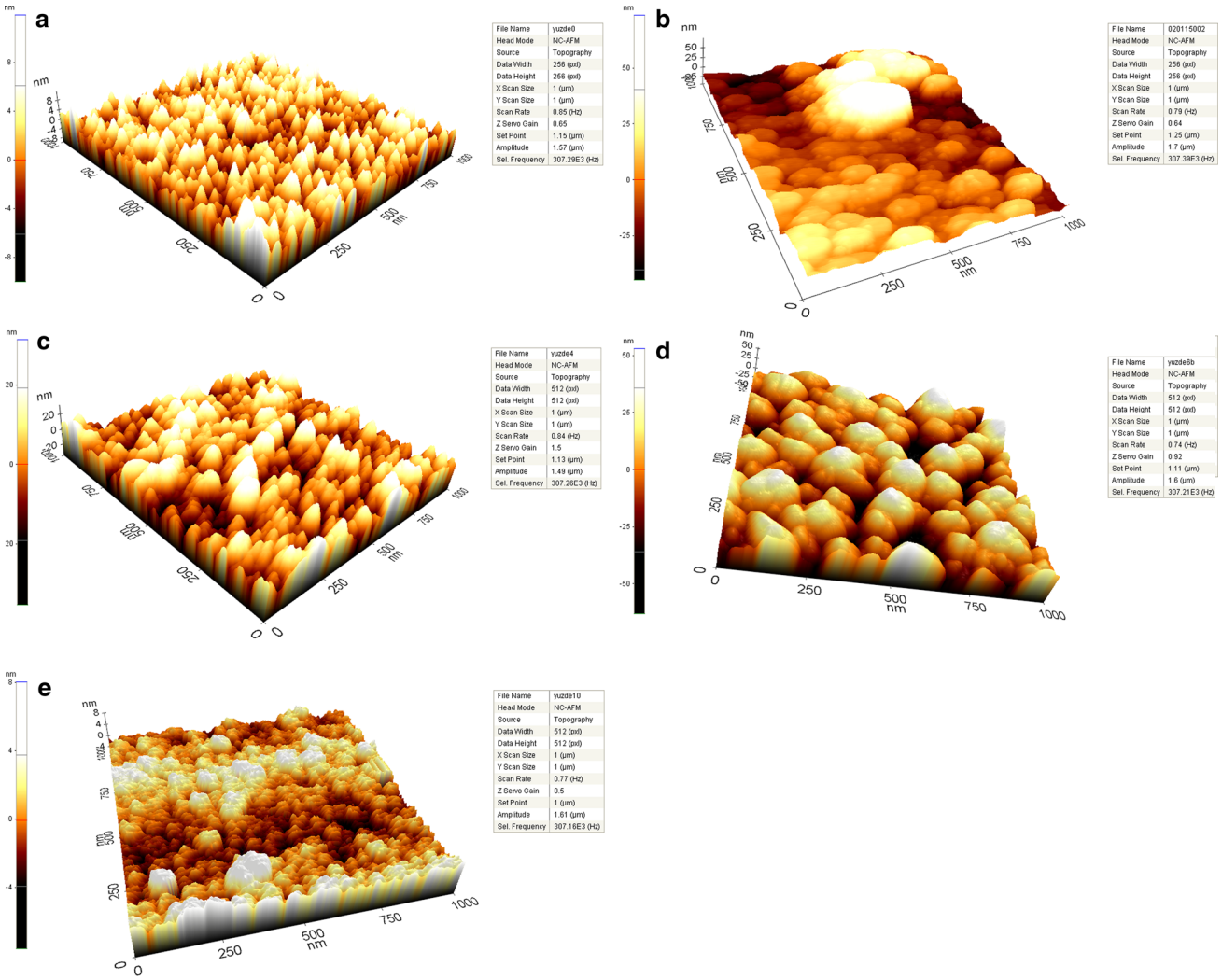

Fig. 4 1 μm × 1 μm AFM images of **a** undoped CuO film, **b** 2 % Ni-doped CuO film, **c** 4 % Ni-doped CuO film, **d** 6 % Ni-doped CuO film, **e** 10 % Ni-doped CuO film

Table 2 Surface roughness values of the undoped and Ni-doped films obtained by AFM

Doping level (%)	Surface roughness (nm)	
	R_a	R_q
0	2.49	3.10
2	19.0	25.0
4	7.75	9.79
6	14.34	1827
10	1.63	2.29

formation of high-quality films. Mageshwari and Sathyamoorthy [28] indicated that the mean grain size increases with the increase in deposition cycles, and as a result, the strain decreases.

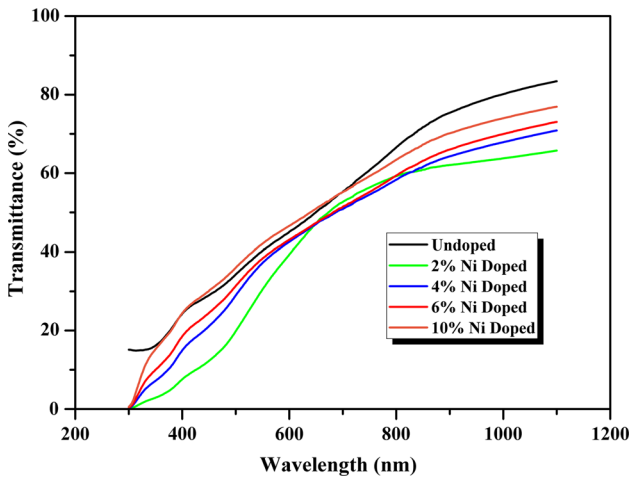

Fig. 5 Transmittance of the films

3.2 Structural analysis

Figure 3 shows SEM images of undoped and Ni-doped CuO films for various doping concentrations grown by the spin-coating technique; uniform, flat film surfaces were revealed, with few defects (e.g. voids or cracks). However, the film surface was covered by nanoparticles (particle diameter: 100 nm), and the coverage rate of the nanoparticles increased with Ni concentration (Fig. 3). The undoped and Ni-doped CuO nanostructured films had nearly the same surface morphology, and they showed plate-like nanostructured films as in [29]. Additionally, the doping concentration of Ni affected the appearance of the film's surface morphology for all films. The film thickness was determined from the cross-sectional view of SEM images; these thicknesses are listed in Table 3.

Figure 4 shows AFM images of undoped CuO and 2, 4, 6, and 10 % Ni-doped CuO thin films at various scales. The figures show a 1 μm × 1 μm area of the films with rod-like particles and a grain structure. The average grain perimeter, determined using XEI software (Park Systems), was 150 nm for the undoped CuO film and 300, 200, 250, and 160 nm for the 2, 4, 6, and 10 % Ni-doped films. The surface roughness of the films (Table 2) was not uniform and did not depend on the doping level. The film structure obtained from AFM images was consistent with the ones obtained from SEM analysis.

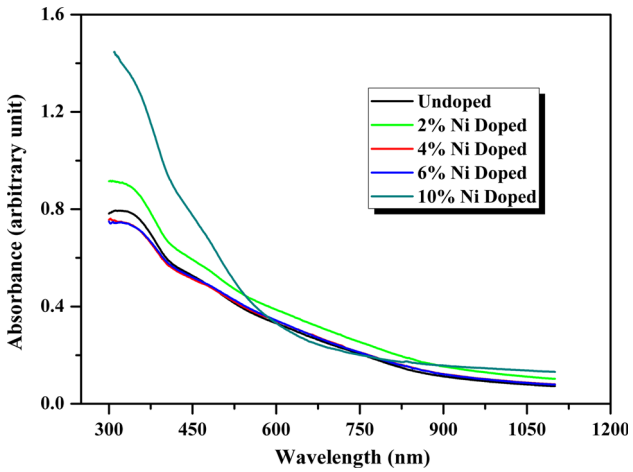

Fig. 6 Absorbance of the films

3.3 Optical properties

The optical transmittance properties of undoped and Ni-doped CuO films annealed at 500 °C are shown in Fig. 5. To study the effect of different doping concentrations on the optical properties, the band gap (E_g), transmittance, and absorption of each film were investigated over the 300- to 1100-nm spectral range. The undoped sample exhibited an average optical transparency of 39.75 % in the visible range. The average transmittance with Ni doping decreased to 30.30 % for the 2 % Ni-doped sample which may be attributed to the increased scattering of photons by crystal defects composed by Ni doping in solution [18] and increased up to 40.97 % for the 10 % Ni-doped sample. Thus, the optical properties of CuO thin films can be modified by Ni doping in the visible range. Figure 6 shows the absorption of the films as a function of the doping concentration. The optical band gap energies were determined using a Tauc plot, by the following equation:

$$\alpha h\nu = \beta\left(h\nu - E_g\right)^m \quad (5)$$

where β is an energy-independent constant, and $h\nu$ is the incident photon energy. m is a constant that determines the type of optical transition; for an indirect allowed transition, $m = 2$; for an indirect forbidden transition, $m = 3$; for a direct allowed transition, $m = 1/2$; and for a direct forbidden transition, $m = 3/2$ [30]. The band gap energy values for the films changed from 2.03 eV with no doping to 2.01 eV, 1.96 eVc, and 1.96 eV with 2, 4, and 6 % Ni doping, respectively; this change was attributed to the band tailing effect [18]. The band gap energy was 2.22 eV for a Ni-doping concentration of 10 %. Similar results were reported in the literature. For example, Srinivasan et al. [31] reported a band gap decrease from 3.83 to 3.53 eV by Zn doping. The decrease in band gap of 2, 4, and 6 % Ni doping shows that the Ni ions are substituted regularly at Cu sites in the CuO nanostructures. The decrease in optical energy band gap (E_g) could be because of the rise of donor density when Ni is

Table 3 Hall effect measurement results of the films

Doping level (%)	Band gap (eV)	Charge concentration (cm^{-3})	Mobility ($cm^2\ V^{-1}\ s^{-1}$)	Resistivity (Ω cm)	Film thickness (μm)
0	2.03	2.16×10^{19}	1.20×10^{-3}	2.35×10^{2}	1.45
2	2.01	1.97×10^{19}	1.22×10^{-3}	2.58×10^{2}	1.48
4	1.96	1.02×10^{18}	2.61×10^{-2}	2.33×10^{2}	1.35
6	1.96	2.32×10^{17}	1.52×10^{-1}	2.22×10^{2}	1.31
10	2.22	6.78×10^{17}	4.38×10^{-2}	2.09×10^{2}	1.22

doped into the CuO nanostructures. The decrease in optical energy band gap may cause the formation of tail-like effect.

3.4 Electrical properties

We investigated the electrical properties of undoped and Ni-doped CuO films using a Hall effect measurement system with van der Pauw configuration at room temperature. A magnetic field of 0.58 T was applied perpendicular with respect to the plane of the sample for the measurement. The Hall coefficient of the films was greater than zero; thus, all of the films exhibited p-type conductivity. Table 3 lists the charge carrier concentration, resistivity, and mobility of the film samples for various doping concentrations. It was seen that the electrical resistivity (ρ) of all films slightly varies with Ni concentration, which may be attributed to the difference in the stoichiometric change induced by more Cu ion vacancies and electrically neutral defects in the surface of films [32]. Drobny and Pulfrey [33] reported an initial increase in electrical resistivity in films for increasing oxygen flow rates. They showed that CuO films with low electrical resistivity associated with non-stoichiometry owing to oxygen vacancies. The charge carrier concentration decreased from 2.16×10^{19} to 6.78×10^{17} cm^{-3} with Ni doping; this change was attributed to the diminishing number of copper vacancies (i.e. the origin of the p-type conductivity). The mobility increased from 1.2×10^{-3} to 4.38×10^{-2} cm^2 V^{-1} s^{-1}, whereas the resistivity did not change significantly with doping concentration. It may be attributed to the improvement in crystallinity of the CuO thin films for different concentrations. Gopalakrishna et al. [34] indicated a significant increase in the mobility of nanostructured CuO thin films after annealing for enhanced ethanol sensitivity. CuO is a low-mobility p-type semiconductor; mobility values of 3.7×10^{-5} cm^2 V^{-1} s^{-1} [35], 6.32×10^{-4} cm^2 V^{-1} s^{-1} [36], and 0.01 cm^2 V^{-1} s^{-1} [37] have been reported in the literature. Higher hole mobility corresponds to lower carrier concentration, due to reduced scattering of holes at the native defects (as self-dopants) [38].

4 Conclusions

High-quality, semi-transparent, p-type Ni-doped CuO films were deposited onto glass substrates using a spin-coating technique; the structural, optical, and electrical properties of these films were studied. XRD spectra revealed that all of the films had a polycrystalline nature, with preferential (002) and (111) orientations. The grain size, dislocation density, and strain of the films as a function of Ni concentration were determined at 500 °C from the value of the FWHM obtained from Scherrer's equation. SEM results indicated that all films were uniform with similar surface roughness. The optical band gap was affected by Ni doping and decreased slightly for 2, 4, and 6 % Ni-doped samples. CuO is a p-type conductive material. Ni doping did not change the conductivity type of CuO; however, the charge carrier concentration decreased by a few orders of magnitude. Thus, we were able to modify the electrical and optical properties of a CuO film using a transition metal dopant, Ni. Our results suggest Ni-doped CuO films as a potential candidate for solar-cell absorber layer applications.

References

1. Yoon KH, Choi WJ, Kang DH (2000) Photoelectrochemical properties of copper oxide thin films coated on an n-Si substrate. Thin Solid Films 372(1):250–256
2. De Los Santos Valladares L, Salinas DH, Dominguez AB, Najarro DA, Khondaker S, Mitrelias T, Barnes C, Aguiar J, Majima Y (2012) Crystallization and electrical resistivity of Cu_2O and CuO obtained by thermal oxidation of Cu thin films on SiO_2/Si substrates. Thin Solid Films 520(20):6368–6374
3. Chang SS, Lee HJ, Park HJ (2005) Photoluminescence properties of spark-processed CuO. Ceram Int 31(3):411–415
4. Han K, Tao M (2009) Electrochemically deposited p–n homojunction cuprous oxide solar cells. Sol Energy Mater Sol Cells 93(1):153–157
5. Steinhauer S, Brunet E, Maier T, Mutinati G, Köck A, Freudenberg O, Gspan C, Grogger W, Neuhold A, Resel R (2013) Gas sensing properties of novel CuO nanowire devices. Sens Actuators B: Chem 187:50–57
6. Tokura Y, Takagi H, Uchida S (1989) A superconducting copper oxide compound with electrons as the charge carriers. Nature 337(6205):345–347
7. Ren G, Hu D, Cheng EW, Vargas-Reus MA, Reip P, Allaker RP (2009) Characterisation of copper oxide nanoparticles for antimicrobial applications. Int J Antimicrob Agents 33(6):587–590
8. Kikuchi N, Tonooka K (2005) Electrical and structural properties of Ni-doped Cu_2O films prepared by pulsed laser deposition. Thin Solid Films 486(1–2):33–37
9. Erdoğan İY, Güllü Ö (2010) Optical and structural properties of CuO nanofilm: its diode application. J Alloy Compd 492(1–2):378–383
10. Al-Kuhaili M (2008) Characterization of copper oxide thin films deposited by the thermal evaporation of cuprous oxide (Cu_2O). Vacuum 82(6):623–629
11. Basith NM, Vijaya JJ, Kennedy LJ, Bououdina M (2014) Structural, morphological, optical, and magnetic properties of Ni-doped CuO nanostructures prepared by a rapid microwave combustion method. Mater Sci Semicond Process 17:110–118
12. Terasako T, Ohmae K, Yamane M, Shirakata S (2014) Carrier transport in undoped CdO films grown by atmospheric-pressure chemical vapor deposition. Thin Solid Films 572:20–27
13. Wang H, Xu JZ, Zhu JJ, Chen HY (2002) Preparation of CuO nanoparticles by microwave irradiation. J Cryst Growth 244(1):88–94
14. Gülen Y, Bayansal F, Şahin B, Çetinkara H, Güder H (2013) Fabrication and characterization of Mn-doped CuO thin films by the SILAR method. Ceram Int 39(6):6475–6480

15. Brazdeikis A, Karlsson UO, Flodström AS (1996) An atomic force microscopy study of thin copper oxide films grown by molecular beam epitaxy on MgO(100). Thin Solid Films 281–282:57–59
16. Ray SC (2001) Preparation of copper oxide thin film by the sol–gel-like dip technique and study of their structural and optical properties. Sol Energy Mater Sol Cells 68(3):307–312
17. Sonia S, Jose Annsi I, Suresh Kumar P, Mangalaraj D, Viswanathan C, Ponpandian N (2015) Hydrothermal synthesis of novel Zn doped CuO nanoflowers as an efficient photodegradation material for textile dyes. Mater Lett 144:127–130
18. Chand P, Gaur A, Kumar A, Kumar Gaur U (2014) Structural and optical study of Li doped CuO thin films on Si (100) substrate deposited by pulsed laser deposition. Appl Surf Sci 307:280–286
19. Bayansal F, Gülen Y, Şahin B, Kahraman S, Çetinkara H (2015) CuO nanostructures grown by the SILAR method: influence of Pb-doping on the morphological, structural and optical properties. J Alloy Compd 619:378–382
20. Mohamed Basith N, Judith Vijaya J, John Kennedy L, Bououdina M (2013) Structural, optical and room-temperature ferromagnetic properties of Fe-doped CuO nanostructures. Phys E 53:193–199
21. Jiang T, Wang Y, Meng D, Wu X, Wang J, Chen J (2014) Controllable fabrication of CuO nanostructure by hydrothermal method and its properties. Appl Surf Sci 311:602–608
22. Huang J, Wu H, Cao D, Wang G (2012) Influence of Ag doped CuO nanosheet arrays on electrochemical behaviors for supercapacitors. Electrochim Acta 75:208–212
23. Dagdelen F, Serbetci Z, Gupta R, Yakuphanoglu F (2012) Preparation of nanostructured Bi-doped CdO thin films by sol–gel spin coating method. Mater Lett 80:127–130
24. Papadimitropoulos G, Vourdas N, Vamvakas VE, Davazoglou D (2006) Optical and structural properties of copper oxide thin films grown by oxidation of metal layers. Thin Solid Films 515(4):2428–2432
25. Alami AH, Allagui A, Alawadhi H (2014) Microstructural and optical studies of CuO thin films prepared by chemical ageing of copper substrate in alkaline ammonia solution. J Alloy Compd 617:542–546
26. Asbrink S, Norrby L-J (1970) A refinement of the crystal structure of copper (II) oxide with a discussion of some exceptional esd's. Acta Crystallogr Sect B: Struct Crystallogr Cryst Chem 26(1):8–15
27. Saleem M, Fang L, Wakeel A, Rashad M, Kong C (2012) Simple preparation and characterization of nano-crystalline Zinc Oxide thin films by sol–gel method on glass substrate
28. Mageshwari K, Sathyamoorthy R (2013) Physical properties of nanocrystalline CuO thin films prepared by the SILAR method. Mat Sci Semicond Proc 16(2):337–343
29. Bayansal F, Şahin B, Yüksel M, Çetinkara HA (2013) SILAR-based growth of nanostructured CuO thin films from alkaline baths containing saccharin as additive. Mater Lett 98:197–200
30. Reddy NK, Reddy KTR (1998) Growth of polycrystalline SnS films by spray pyrolysis. Thin Solid Films 325(1–2):4–6
31. Jayaprakash J, Srinivasan N, Chandrasekaran P, Girija EK (2015) Synthesis and characterization of cluster of grapes like pure and Zinc-doped CuO nanoparticles by sol–gel method. Spectrochim Acta Part A: Mol Biomol Spectrosc 136:1803–1806
32. Ogwu A, Darma T, Bouquerel E (2007) Electrical resistivity of copper oxide thin films prepared by reactive magnetron sputtering. J Achiev Mater Manuf Eng 24(1):172–177
33. Drobny V, Pulfrey L (1979) Properties of reactively-sputtered copper oxide thin films. Thin Solid Films 61(1):89–98
34. Gopalakrishna D, Vijayalakshmi K, Ravidhas C (2013) Effect of annealing on the properties of nanostructured CuO thin films for enhanced ethanol sensitivity. Ceram Int 39(7):7685–7691
35. Jundale DM, Joshi PB, Sen S, Patil VB (2012) Nanocrystalline CuO thin films: synthesis, microstructural and optoelectronic properties. J Mater Sci: Mater Electron 23(8):1492–1499
36. Gonçalves A, Campos L, Ferlauto A, Lacerda R (2009) On the growth and electrical characterization of CuO nanowires by thermal oxidation. J Appl Phys 106(3):034303
37. Sanal KC, Vikas LS, Jayaraj MK (2014) Room temperature deposited transparent p-channel CuO thin film transistors. Appl Surf Sci 297:153–157
38. Shen Y, Guo M, Xia X, Shao G (2015) Role of materials chemistry on the electrical/electronic properties of CuO thin films. Acta Mater 85:122–131